Coherence of large gratings and electronbeam fabrication techniques for atomwave interferometry

Michael J. Rooks, Richard C. Tiberio, Michael Chapman, Troy Hammond, Edward Smith et al.

Additional information on J. Vac. Sci. Technol. B

Coherence of large gratings and electron-beam fabrication techniques for atom-wave interferometry

Michael J. Rooks and Richard C. Tiberio
National Nanofabrication Facility at Cornell University, Ithaca, New York 14853

Michael Chapman, Troy Hammond, Edward Smith, Alan Lenef, Richard Rubenstein, and David Pritchard
Department of Physics, Massachusetts Institute of Technology, Cambridge, Massachusetts 02139

Scott Adams
Department of Theoretical and Applied Mechanics, Cornell University, Ithaca, New York 14853

We describe the fabrication of slotted, free-standing structures used as amplitude gratings in a separated-beam interferometer. Improvements in electron-beam writing techniques have allowed us to compensate for electron-beam system drift, making practical the exposure of 800×800 μm gratings with period as small as 0.14 μm. Alignment marks are used for periodic drift compensation. Finite element analysis of fracture formation in silicon nitride films gives us a tool for the prediction of structural failure in arbitrarily shaped free-standing structures. © *1995 American Vacuum Society.*

I. INTRODUCTION

The field of atom optics and atom interferometry has grown rapidly since the development of optical elements based on the manipulation of atoms with light[1] or with physical gratings.[2] This article describes the fabrication of slotted, free-standing structures used as amplitude gratings in a separated-beam interferometer. Atom interferometry has allowed the measurement of the index of refraction of atoms and dimer molecules traveling through gases,[3] as well as measurements of magnetic substates[4] and the electric polarizability of sodium.[5]

The critical optical element for this interferometer is the free-standing grating. Interference contrast relies on the grating being coherent over its length, with minimal distortions induced by stress. The goal of the fabrication process is to produce gratings whose phase remains in step to within a fraction of the grating period. Grating lines must be straight to the order of their linewidth over their length, and the grating period must be constant to the order of the grating period over the width of the grating (or, over the width of the atomic beam, whichever is smaller). Holographic lithography is capable of generating such highly coherent gratings over large areas and has been used to fabricate silicon nitride gratings similar, but much larger than ours.[6] Holography has the disadvantage (over electron-beam lithography) that patterns are limited to straight gratings, and that support structures must be defined in a separate step. The electron-beam lithography techniques reported here can be applied to any pattern, and in theory can be scaled to narrow structures with lengths on the order of 50 cm. In the future, a combination of electron-beam and holographic techniques[7] may provide the optimal combination of coherence and versatility.

We have previously reported the fabrication and characterization of 0.4 μm period gratings.[8] In this article we describe new fabrication methods for decreasing the grating period to 0.14 μm, for increasing the area to 800×800 μm^2 and for improving the coherence of gratings.

II. FABRICATION

The fabrication process (see Fig. 1) begins with the deposition of low-stress silicon nitride. Silicon wafers ($\langle 100 \rangle$, 3 in. diameter, 250 μm thick) are cleaned with the standard RCA process.[9] To remove any surface defects, the wafers are then oxidized, and the oxide is stripped in buffered oxide etchant (HF:H$_2$O 1:10 with ammonium fluoride). Wafers are then coated on both sides with amorphous silicon nitride, deposited by low-pressure chemical vapor deposition (LPCVD) using gas sources of dichlorosilane (SiH$_2$Cl$_2$) and ammonia (NH$_3$). Low-stress, nonstoichiometric silicon, nitride films were formed by using a mixture rich in dichlorosilane, SiH$_2$Cl$_2$:NH$_3$ of 4.27:1 at a deposition temperature of 850 °C. Silicon nitride produced with this process is stiff (elastic modulus $\sim 3 \times 10^{11}$ Pa) and has low residual stress (~ 300 MPa). Low-stress silicon nitride has about one-tenth the internal stress and about one-half the tensile strength of stoichiometric silicon nitride (Si$_3$N$_4$).

Free-standing, unpatterned silicon nitride films ("windows") are made by first patterning the silicon nitride on the backside of a wafer. The photoresist is exposed, developed, and used as a etch mask for reactive ion etching (RIE) in CF$_4$. The silicon is etched in 4 M KOH (93 °C), which etches Si 50 times faster in the $\langle 100 \rangle$ direction than it does in the $\langle 111 \rangle$ direction. Since the KOH etches slowly in the $\langle 111 \rangle$ direction, the last traces of silicon left on the silicon nitride windows are small pyramids which etch very slowly. To speed the process we remove the wafers from the KOH solution, rinse thoroughly in water, and finish the etch with an acid mixture (HNO$_3$:HF:H$_2$O 150:8:75) which etches silicon isotropically. The isotropic etch eliminates sharp, jagged silicon edges which form when rectangular windows are misaligned with respect to the crystal plane. Trimble *et al.*[10] have reported that this final isotropic etch rounds out the corners of the silicon, thus avoiding sharp edges which could break the nitride. Our results are consistent with this, since our yield has been greatly improved by the technique.
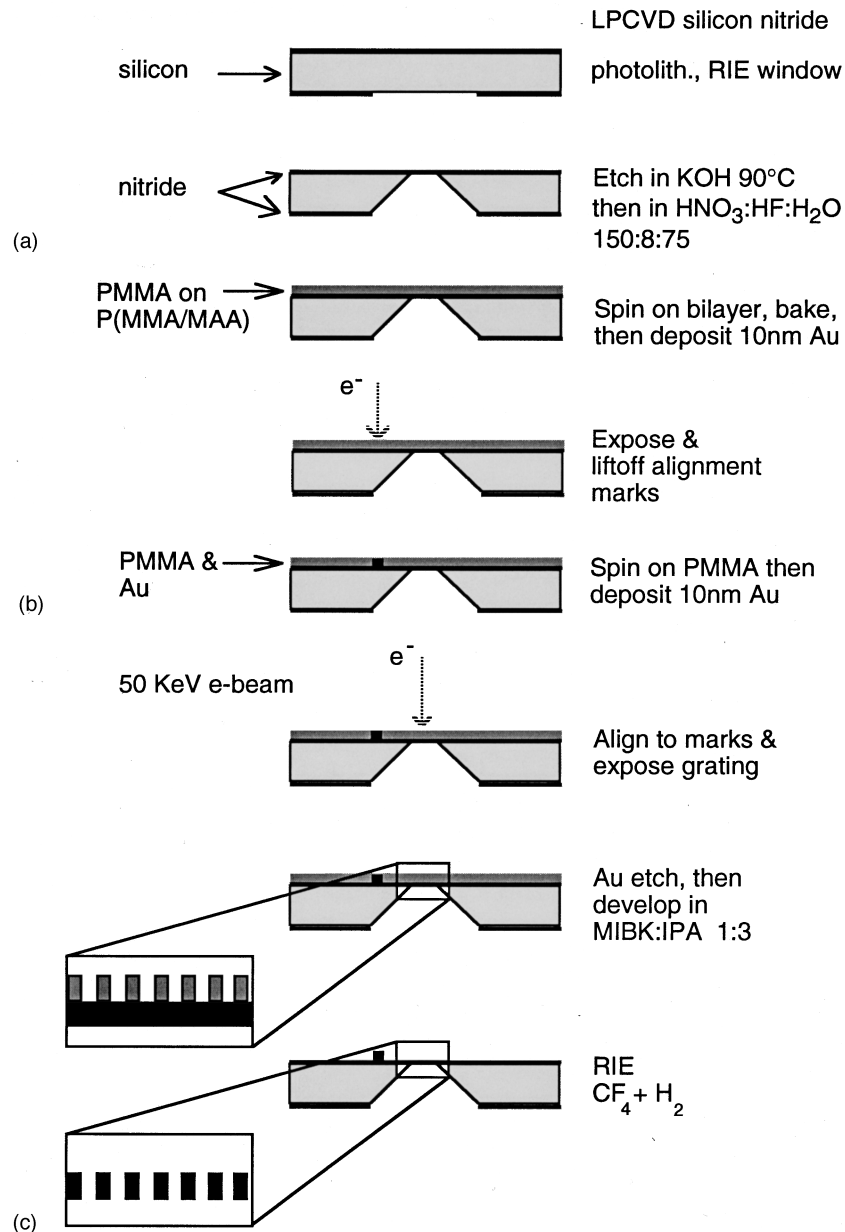
FIG. 1. Grating fabrication sequence. Silicon wafers are cleaned, then coated by LPCVD with low-stress silicon nitride. The "window" pattern is printed in photoresist, then etched into the nitride with RIE in CF_4. The window pattern is etched through the silicon wafer with KOH, then with a mixture of acids. The first e-beam exposure defines gold alignment marks. In the second e-beam step, the marks are used for alignment, and gratings are written over the windows. The PMMA resist is then used as a mask for etching the nitride in CF_4 and H_2.

After preparing the windows, the wafer is spin-coated with ∼170 nm of PMMA, baked for 1 h at 170 °C and coated with 10 nm of Au. The Au is needed for charge dissipation during electron-beam patterning. After exposure the Au is removed with a KI/I mixture,[11] and the exposed PMMA is developed with methyl isobutyl ketone and isopropanol (MIBK:IPA, 1:3). Gratings are exposed with 50 keV electrons using a JEOL JBX-5DII lithography system.

Gratings exposed in PMMA are used directly as the mask for RIE of silicon nitride in CF_4 and H_2. Normally PMMA offers poor selectivity for plasma etching, and a layer much thicker than the nitride would be required. However, a nitride thickness of 150 nm and a grating period of 140 nm require a PMMA aspect ratio greater than 2:1. To maintain good edge acuity and a reasonable PMMA aspect ratio we require an etch selectivity of at least 1:1. We have developed a selective RIE chemistry by adding a polymerization promoter, H_2, to the fluorine-based etchant, CF_4. Our process uses 5 sccm of H_2 and 42 sccm of CF_4 at a pressure of 15 mTorr and dc self-bias of 300 V. Silicon nitride etches at 28 nm/min, and PMMA etches at roughly the same rate. Increasing the amount of H_2 causes the PMMA etch rate to drop, and improves the selectivity; however, the etch rate becomes less consistent, due to polymer deposition on the walls of the chamber. Higher flows of H_2 can lead to a net deposition of polymer on the sample. Another important consideration is that PMMA will flow when heated above its glass transition temperature, 110 °C. To avoid PMMA flow, the nitride is

etched in 2–3 min cycles with 2 min of cooling between etch step. This etch recipe has proven to be equally effective when etching silicon dioxide.[12]

III. SOURCES OF INCOHERENCE

Gratings are written with 50 keV electrons, using a JEOL JBX-5DII electron-beam (e-beam) system with a LaB_6 emitter and a stage controller accurate to $\lambda/128$ (5 nm). The beam is focused to a ~20 nm spot in a 80×80 μm writing field. Grating coherence is compromised by a number of factors:

(1) Vibration and misalignment in the interferometer: We have verified that vibrational noise from the necessary nearby roughing pumps and, to a lesser extent, from water flow in the diffusion pump cooling lines causes a degradation in the atom interferometer fringe contrast. By briefly turning off some of the noise sources, fringes were obtained with approximately 10% higher contrast. A combination of suspending the interferometer and/or the pumps may isolate the interferometer from most of the vibrational building noise.

(2) Roughness and continuity of the individual lines affects the interferometer's fringe contrast, but is less important than the overall coherence of the grating.

(3) Distortions in the writing field caused by nonlinear deflection can be compensated on our e-beam tool with the use of a hardware distortion map. We have found that, even with extensive averaging of the calibration data, the deflection distortions in a 80 μm field are below the noise of the mark detection electronics; that is, less than 5 nm.

(4) Writing field stitching errors are caused by imperfect calibration of the beam deflection. These errors, due to incorrect field sizing and rotation, arise either due to mark detection inaccuracy, or because the substrate is not perfectly planar. A substrate which is 1 μm out of the plane will cause a field sizing error of 4 nm (assuming a 10 mm working distance and a field size of 80 μm). By careful calibration of the deflection gain and field rotation using marks on the substrate, field-to-field stitching errors are kept in the range of 10–15 nm.

(5) Stitching errors are also caused by stage roll, pitch, and yaw (rotation of the stage about the X, Y, and Z axes, respectively). Stitching errors are measured by writing verniers at the intersections of writing fields.

(6) Drift in electronics or temperature changes in the e-beam column will cause random shifts in the deflection origin. Drift is measured by writing one side of a vernier before writing the grating, then writing the matching vernier pattern after the grating.

(7) The silicon wafer may change temperature during e-beam patterning, causing a gradual drift due to thermal expansion. While this effect could accumulate several microns of error, it can be avoided by allowing the substrate to come to thermal equilibrium before exposure. It is difficult to distinguish this thermal shift from drift in the electronics or temperature changes in the column.

Of these sources of incoherence, errors due to stage roll, pitch, and yaw are the hardest to characterize. These so-called runout errors in an e-beam tool are caused by slow changes in orthogonality over the length of the stage. Standard laser-controlled stages correct only for deviations in X and Y, but not for any angular errors.[13] While runout errors contribute to field-to-field stitching errors, the dominant effects may be drift and calibration error. A significant runout error of 0.1 μm over a 2000-μm-long grating would cause an average field-to-field stitching error of 4 nm; this error is difficult to measure with vernier matching patterns. The technique used to measure drift (writing matching verniers before and after the grating) will not work for measuring runout errors, since the systematic errors incurred during forward travel will be exactly reversed upon return to the vernier's origin. For the production of large commercial mask plates, the operational solution to this problem has been to characterize one e-beam system with respect to another. Similarly, one could characterize the X axis with respect to the Y axis by writing a horizontal set of marks, turning the substrate 90°, then measuring the mark locations with the same system. In any case, the measured runout is a convolution of two values. It is clear that a more absolute measure of stage runout would be valuable. Since no such measure is currently available, the stage runout is observable only as part of the net loss of contrast in the atom interferometer.

If field-to-field stitching errors (in our case, 10–15 nm) are dominated by calibration errors (for instance, an incorrect measure of field rotation) or by drift, then why is runout at all important? Imagine a runout error which oscillates over the length of the grating, with an amplitude comparable to the grating period. This runout will degrade the coherence significantly, yet the stitching error at each field boundary may be too small to measure. On the other hand, a random drift error (say, on the order of 10% of the grating period) will cause a much larger field stitching error, even though a fit to a straight line would show that the overall coherence is not as compromised.

IV. COMPENSATION TECHNIQUES

Drift in system electronics can be measured by writing one side of a vernier before the grating, and the matching half after the main exposure. Over an exposure time of 10–15 min, we find that the system will drift around 50–60 nm. By repeatedly measuring the location of one mark over several hours, we find that the system drifts in a random walk pattern with a net drift on the order of 0.1 μm in 1 h. We have compensated for system drift by periodically aligning to marks placed along the grating every 160 μm. The marks are placed around 50 μm from the center of the grating, depending on the width of the silicon nitride window. The e-beam system's stage is moved so that an alignment mark is in the center of the writing field, and the mark's position is measured automatically by scanning the beam. The stage is then moved back to a writing position over the silicon nitride window. Stage motion is minimized to avoid stage motion (runout) errors after alignment. Cross-shaped Au marks are patterned next to the nitride windows, using a high-speed process. These marks are patterned with the same e-beam tool, with an exposure time of 3 s to write all of the marks for a single millimeter-long grating. Because the marks are written in the center of writing fields, errors from

imperfect deflection and rotation calibration do not influence the pattern. The marks are affected by the same runout errors affecting the gratings, but system drift can be effectively eliminated. In addition to their use for drift compensation, marks on the silicon wafer are used to calibrate the field gain and rotation, thereby reducing errors arising from the use of marks on the stage, marks which are not in the same plane as the substrate.

A technique commonly used to relieve stitching errors on mask plates is to overlap the pattern at field boundaries. We take this idea further, by overlapping 80 μm fields every 16 μm. In this way each line of the grating is exposed five times, each time at $\frac{1}{5}$ of the total dose, from five different locations in the field. Under normal operating conditions the 80 μm writing fields are divided into a uniform grid of smaller sections called "subfields" (usually $\sim 10 \times 10$ μm) so that features inside each subfield can be patterned with high-speed 12-bit digital-to-analog converters (DACs). 16-bit DACs are used to place the origin of each subfield. We use ten different subfield sizes, so that any subfield (interfield) placement errors will also be randomized. By overlapping fields we average the stitching error over the length of a writing field, turning random placement errors into slightly increased linewidth. Stitching errors due to systematic problems (nonplanar sample, stage runout, and calibration error) are converted from sudden shifts of high spatial frequency into gradual shifts of low spatial frequency. We have used this technique for the production of laser distributed–feedback/distributed Bragg reflector (DFB/DBR) gratings, but have not yet applied the method to the fabrication of atom interferometer gratings.

V. FRACTURE SIMULATION

We have found empirically that gratings are most stable when the pattern includes support lines 1 μm wide perpendicular to the fine grating, with a period of 4 μm (see Fig. 2). Also, gratings are far less likely to break if they are written over the entire nitride window, instead of just in the center. To understand these empirical observations and to better predict the catastrophic failure of free-standing structures, we have conducted simulations of crack formation in silicon nitride films. To test the simulations, wafers were prepared as above (150 nm of low-stress silicon nitride), with a large set of 1×1 mm silicon nitride windows. Patterns of varying shape were written over the wafer to observe the point at which the windows would break. The membranes fail as the holes are etched through the nitride; no external strain is applied to the window.[14]

Two different structures were patterned to test the simulation: a single slot in the center of a window and a grating across a window. In the former case, the length of the slot (one in each window) was varied from 2 to 20 μm, with a fixed width of 0.1 μm. As the length of the slot is increased, the magnitude of the stress concentration at the ends of the slot is increased. At a critical stress level, a crack propagates from the end of the slot, and the window is destroyed. In the latter case, the grating lines had a fixed length of 5 μm, a fixed width of 0.1 μm, and a 1 μm support structure (similar to the atom interferometer grating). In this case the period of
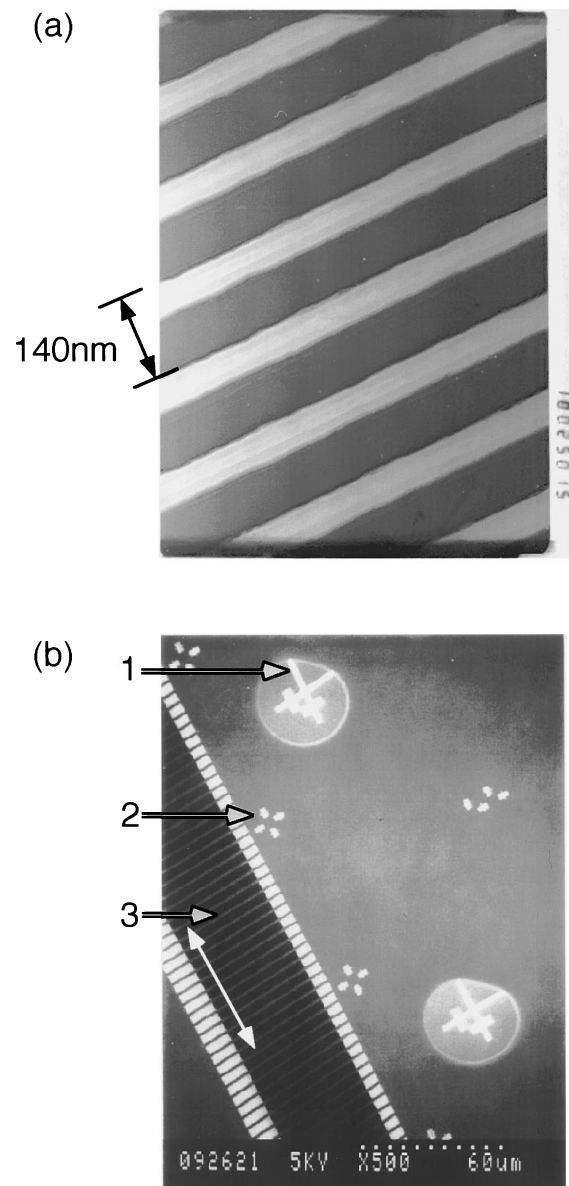

FIG. 2. Gratings used for the atom interferometer. (a) TEM micrograph of a 140 nm period grating. The light areas are low-stress silicon nitride. Grating lines are 3 μm long between support structures. The film is 150 nm thick. (b) Lower magnification view of the completed grating, showing (1) cross-shaped Au alignment mark, with cross-linked PMMA left on two of the arms from the alignment scan, (2) verniers at writing field intersections, and (3) the grating on a silicon nitride window. The dark region (3) is the window; the grating overlaps onto the solid silicon. Diagonal lines over the window are the 4 μm period support grid. Fine grating lines are parallel to the double-ended arrow (inserted).

the grating was varied between 0.2 and 20 μm. When the period becomes larger, the stress relief produced by the adjacent cracks is reduced. Similar to the former case, cracks propagate at a critical value of the period, and the window is destroyed. Figure 3 shows the plot of the percentage of broken windows versus the slot length (for the first case) and versus grating period.

We simulated the single-slot and grating experiments using EPFRANC2D (elastic-plastic fracture analysis code, two dimensions), an interactive finite element code that is ca-
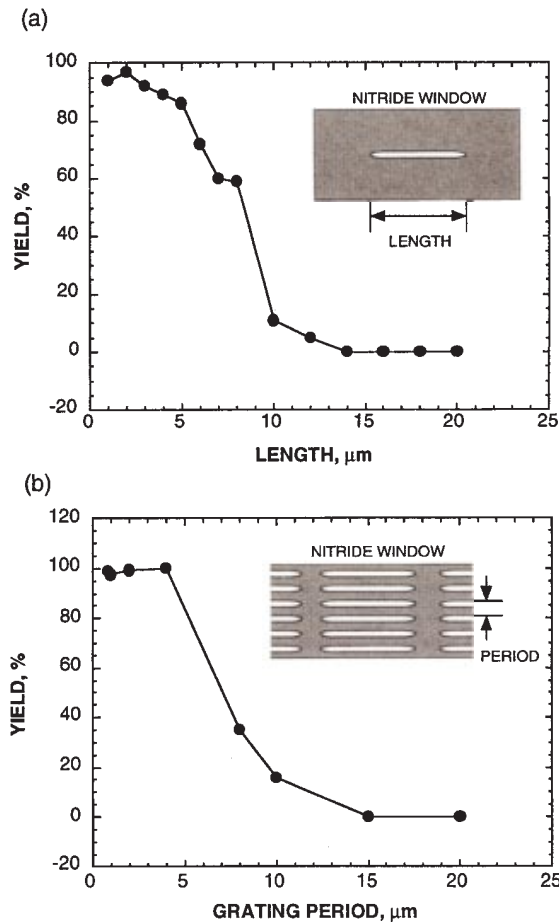
(a)

(b)

FIG. 3. Yield of test structures is measured to extract the value of the stress coefficient K_{IC}. Patterns of holes are etched into 150-nm-thick low-stress silicon nitride windows, each 1×1 mm. (a) A single 0.1-μm-wide line is etched into each window, and the length of the line is varied across the wafer. When the line length exceeds ~ 8 μm, most of the windows break. (b) Grating lines of fixed length 5 μm (1 μm support bars between lines) have a pitch which varies between 0.5 and 20 μm. When the grating pitch exceeds ~ 7 μm, most of the windows break.

pable of performing fracture mechanics analyses of two-dimensional structures.[15] One goal of these simulations was to show a correlation between the stresses present in the single-slot geometry and those of a grating geometry that exhibited catastrophic failure during fabrication. The criteria that we used to compare the critical geometries was based on the mode I stress intensity factors present in each case.[16] Assuming that the single slot and the grating slots are sharp cracks, we used the stress criterion for crack propagation that states that a crack will propagate if the stress intensity factor exceeds a critical value, i.e., the plane strain fracture toughness for mode I. Failure was assumed to occur when any crack tip began to propagate.

The far field membrane stress was simulated by restraining the boundary of the window from all motions and assigning a temperature drop and coefficient of thermal expansion which resulted in the measured membrane stress. Figure 4(a) shows a typical deformed finite element mesh for the grating experiment. The corresponding plot of the maximum principle stresses present in this case is shown in Fig. 4(b). In order to invoke the stress criterion for crack propagation, the
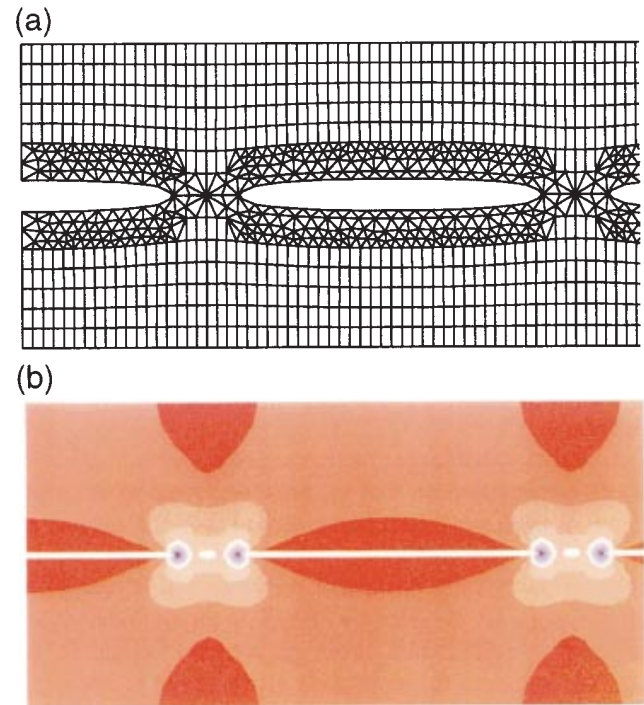
(a)

(b)

FIG. 4. (a) Magnified view of a portion of the finite element mesh used in the grating simulations. The mesh is deformed due to membrane stresses simulated using thermal loading. The deformation is magnified; its largest value is 1 nm. The top and bottom surfaces were restrained from motion in the vertical direction to impose symmetric boundary conditions. The left-most edge was restrained from motion in the horizontal direction for similar reasons. (b) Plot of the maximum principle stresses present in the grating structure. Red corresponds to the lowest principle stress, and dark blue, the highest.

crack tip must be predominantly under a state of plain strain. Experimental results have shown that if the following condition is met, the crack tip is sufficiently in this state of plain strain:[17]

$$\text{nitride thickness} \geq 2.5 (K_{IC}/\sigma_{\text{yield}})^2,$$

where K_{IC} is the mode I fracture toughness and σ_{yield} is the yield stress of the material, approximately 10 GPa. By choosing a single-slot geometry which corresponded to the design where 50% of the single slots failed, we estimated the mean plane strain fracture toughness to be 1.08 MPa m$^{1/2}$ from the formula

$$K_{IC} = \sigma_c \sqrt{\pi a},$$

where the membrane stress σ_c equals 300 Mpa, and a, one-half of the crack length, equals 4.2 μm. Using these results, the film thickness must be greater than 59 nm to be in a state of plane strain. This thickness is well below the 150 nm film thickness used in these experiments.

In order to compare experimental results and to establish the critical stress intensity factor (SIF) range for membrane failure, simulations were run on the single slot and grating geometries. Using the single-slot geometry, all of the silicon nitride windows broke (zero yield) when the slots were made 14 μm long. In this case the simulated SIF was 1.31 MPa (m)$^{1/2}$. Using the grating geometry, 15 μm period gratings had zero yield, with a simulated SIF of 0.87 MPa (m)$^{1/2}$.

In these cases, patterns with equal yields have stress intensity factors which differ by roughly 40%. Qualitatively, this difference can be partly attributed to the fact that the fracture toughness of a material is not a specific value, but a distribution. In the case of the single-slot experiment, there are only two cracks. In the grating experiments, there are approximately 2000 crack tips. Even a high survival probability for a single crack may result in a very small survival probability for a pattern with multiple cracks. For a quantitative explanation, analyses need to be performed where the loading is controlled more precisely using techniques such as the bulge test[14] or cooling tests which rely on the mismatch in thermal expansion of the silicon substrate and the nitride membrane.

It is quite possible that fabrication steps contain an important failure mechanism that we have neglected in our simulations. As the pattern is being etched into the nitride, the film is being subjected to a dynamic load. Due to nonuniformities in the etching process, some slots will be completed before others. As the slots are etched through the membrane, the rapidly redistributed stress may cause failure. In any case, the results of the simulation give a rough bound on the stress intensity factors that should be avoided. The benefit of using a program such as EPFRANC2D is the ability to compare arbitrary geometries, using the stress intensity factors as a means of comparison.

There are many desired geometries where the stress intensity factor would exceed the fracture toughness of the nitride membrane and result in catastrophic failure. Using EPFRANC2D, stress relief techniques can be explored before the structures are fabricated. Examples of these techniques include the formation of narrow (0.1 mm) slots and holes to shield the tips of larger cracklike structures. If necessary the stress relief structures may later be filled in by the direct deposition of a low-stress material.

VI. RESULTS

Gratings of period 0.2 μm written using periodic alignment have provided a relative improvement of 20% in the contrast of fringes in the atom interferometer. Coupled with the elimination of roughing pump and water line noise, a total relative improvement in fringe contrast of 60% was achieved. Fringes with 43% contrast are observed, compared to previous typical fringes of 27%. The maximum theoretical contrast in our interferometer depends somewhat on the particular open fractions of the three gratings and is usually in the range of 65%–70%. It is important to note that we are now able to achieve the stated high contrast with large areas of the grating being used. With gratings made under older procedures, the beam height and/or width usually needed to be restricted to obtain maximum contrast.

We have now verified that with the new gratings, the entire height of the grating can be used with no significant loss of contrast. Previously, the highest contrast fringes were obtained by reducing the height of the beam and thus reducing the total area of the grating that must be phase coherent. This verifies that the lines from one writing field to the next are parallel to a very high degree.

The new, large area, 800$\times$800 μm slits written with periodic alignment have allowed us to study the effect of removing the collimating slits and using a very wide atomic beam. Just as in the case of gratings over narrow windows, marks next to the wide windows are used for alignment. The stage is moved to the closest mark, and after alignment is moved back to the patterning location. Gratings on large windows give us a test of coherence in the direction perpendicular to the grating lines, where any stitching errors would cause the grating phase to jump discretely. Removing the collimating slits in our apparatus complicates the calculation of expected fringe contrast. Various diffracted orders or "ports" of our interferometer that were cleanly separated now overlap. Since some of these are interfering orders and others are not, the overlap causes a reduction in the expected contrast. For the particular configuration we used, we expected a decrease in the fringe contrast of a factor of 2.0; instead we observed a decrease by a factor of 2.3. There are other effects, including nonoptimal placement of the diffraction gratings, that could have a small effect on the contrast when the collimation slits are removed. However, assuming that the gratings are responsible for the remaining coherence loss, we can place a stringent upper bound on the contrast loss due to grating imperfections.

The coherence that we have observed in these large-area gratings is promising. It should allow larger beams to be used with little loss in contrast—a tremendous gain in the signal-to-noise ratio for atom interferometers. In addition, slower atomic beams and beams with lighter atoms—both of which have a longer wavelength—require larger gratings to encompass the larger diffraction angle. Finally, large-area gratings will also be required for high precision measurement of inertial effects (acceleration and rotation). These measurements require the maximum possible atom flux at the detector.

VII. CONCLUSIONS

We have achieved improved performance of the atom interferometer through the use of periodic alignment for drift compensation during e-beam patterning. This technique has allowed us to compensate for system drift, making practical the exposure of large 800$\times$800 μm gratings. Larger gratings will also be practical, by using higher-speed resists and/or higher-brightness (field emission) electron sources. The use of overlapping fields ("voting" lithography) is expected to eliminate errors with high spatial frequencies, trading linewidth for field stitching errors.

Placement errors due to drift, calibration errors, and nonplanar substrates are measured with verniers, but low-frequency stage runout errors cannot be measured without some independent reference of absolute position. Holographic gratings may provide such a reference, with a simple analysis up to a size scale of 1–2 cm. Beyond this size, holographic gratings do not maintain a linear phase relation[17] and so the interpretation of stage metrology becomes more complex, requiring a knowledge of the holographic grating's center.

Future development of high-speed, compact atom interferometers will benefit from the characterization and compen-

sation of placement errors in electron-beam lithography. Other devices—such as long channel-dropping filters, DFB laser gratings, and large Fresnel lenses—face the same problems in the fabrication of coherent structures.

Simulation of fracture formation in silicon nitride films has given us a tool for the prediction of structures that will fail during fabrication, and a way of evaluating stress relief patterns in arbitrary structures. We have used two sets of simple patterns to identify the critical stress intensity factors in thin, free-standing films of nonstoichiometric silicon nitride.

ACKNOWLEDGMENTS

[1] F. Riehle, T. Kisters, A. Whitte, J. Helmcke, and C. J. Bordé, Phys. Rev. Lett. **67**, 117 (1991).

[2] J. Schmiedmayer, C. R. Ekstrom, M. S. Chapman, T. D. Hammond, and D. E. Pritchard, in *Fundamentals of Quantum Optics III*, edited by F. Ehlotzky (Springer, Berlin, 1993).

[3] J. Schmeidmayer, M. Chapman, C. Ekstrom, T. Hammond, S. Wehinger, and D. Pritchard, Phys. Rev. Lett. **74**, 1043 (1995); M. Chapman, C. Ekstrom, T. Hammond, R. Rubenstein, J. Schmeidmayer, S. Wehinger, and D. Pritchard, *ibid.* (to be published).

[4] J. Schmeidmayer, C. Ekstrom, M. Chapman, T. Hammond, and D. Pritchard, J. Phys. II (France) **4**, 2029 (1994).

[5] C. Ekstrom, J. Schmeidmayer, M. Chapman, T. Hammond, and D. Pritchard, Phys. Rev. A (to be published).

[6] J. M. Carter, D. B. Olster, M. L. Schattenburg, A. Yen, and H. I. Smith, J. Vac. Sci. Technol. B **10**, 2909 (1992).

[7] V. V. Wong *et al.*, J. Vac. Sci. Technol. B **12**, 3741 (1994).

[8] D. W. Keith, R. J. Soave, and M. J. Rooks, J. Vac. Sci. Technol. B **9**, 2846 (1991).

[9] W. Kern, J. Electrochem. Soc. **137**, 1887 (1990).

[10] L. E. Trimble, G. K. Celler, J. Frackoviak, and G. R. Weber, J. Vac. Sci. Technol. B **10**, 3200 (1992).

[11] Gold etch solution type TFA from Transene Co., Rowley, MA.

[12] W. C. B. Peatman, P. A. D. Wood, D. Porterfield, T. W. Crowe, and M. J. Rooks, Appl. Phys. Lett. **61**, 294 (1992).

[13] The exception to this is a stage built at IBM which corrects for yaw. See R. Kendall, S. Doran, and E. Weissmann, J. Vac. Sci. Technol. B **9**, 3019 (1991).

[14] A more extensive study of fracture strength has been conducted by J. A. Liddle *et al.*, using a bulge test in which a membrane is pressurized until it fractures. See J. A. Liddle, H. A. Huggins, P. Mulgrew, L. R. Harriott, H. H. Wade, and K. Bolan, in *Materials Reliability in Microelectronics IV*, Proc. Mater. Res. Soc. (Materials Research Society, Pittsburgh, 1994).

[15] P. Wawrzynek and A. Ingraffea, NASA Contractor Report 4572.

[16] Broek, David, *Elementary Engineering Fracture Mechanics* (Kluwer Academic, Hingham, MA, 1986).

[17] E. H. Anderson, V. Boegli, M. K. Schattenburg, and H. I. Smith, J. Vac. Sci. Technol. B **9**, 3606 (1991); H. I. Smith, IEEE Proc. **62**, 1361 (1974).